Electronic Supplementary Material (ESI) for Nanoscale.
This journal is © The Royal Society of Chemistry 2020

Supporting Information

Boosting the Potassium Storage Performance via Functional Design of Heterostructure Bi_2S_3@RGO Composite

Yuhan Liu[a], Malin Li[*a,b,], Yingying Zheng[c], Hezhe Lin[a], Ziyang Wang[a], Wen Xin[a], Chunzhong Wang[a] and Fei Du[*a]

[a] *Key Laboratory of Physics and Technology for Advanced Batteries (Ministry of Education), College of Physics, Jilin University, Changchun 130012, P. R. China*

[b] *State Key Laboratory of Inorganic Synthesis and Preparative Chemistry, College of Chemistry, Jilin University, Changchun 130012, P. R. China*

[c] *Key Laboratory of Automobile Materials (Ministry of Education), College of Materials Science and Engineering, Jilin University, Changchun, 130012, PR China*

*Correspondence to: malinl@jlu.edu.cn, dufei@jlu.edu.cn

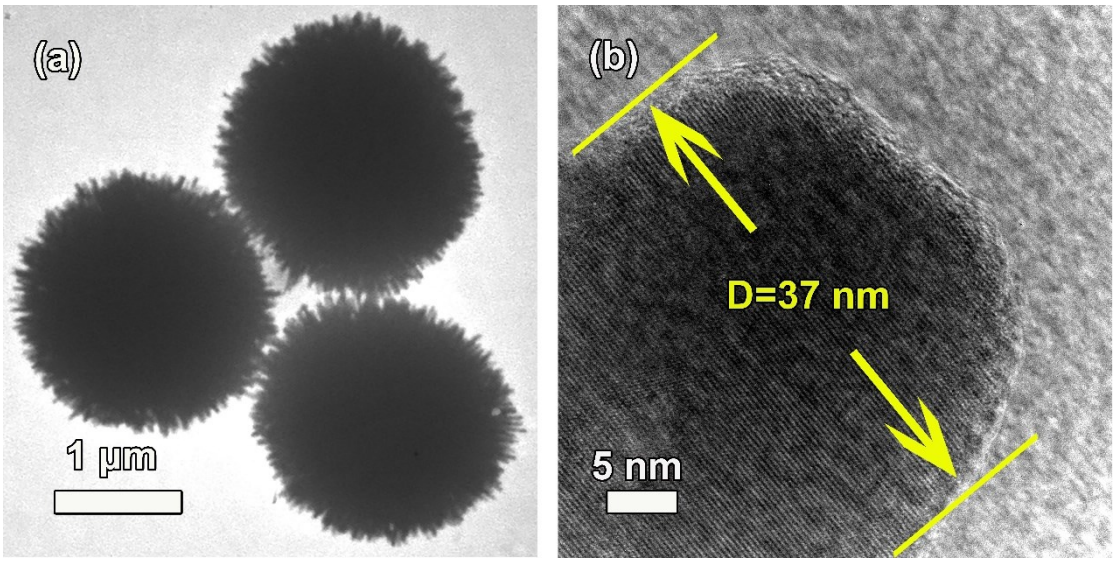

Fig. S1 (a) TEM images and (b) HRTEM image of self-assembled Bi_2S_3 microspheres.

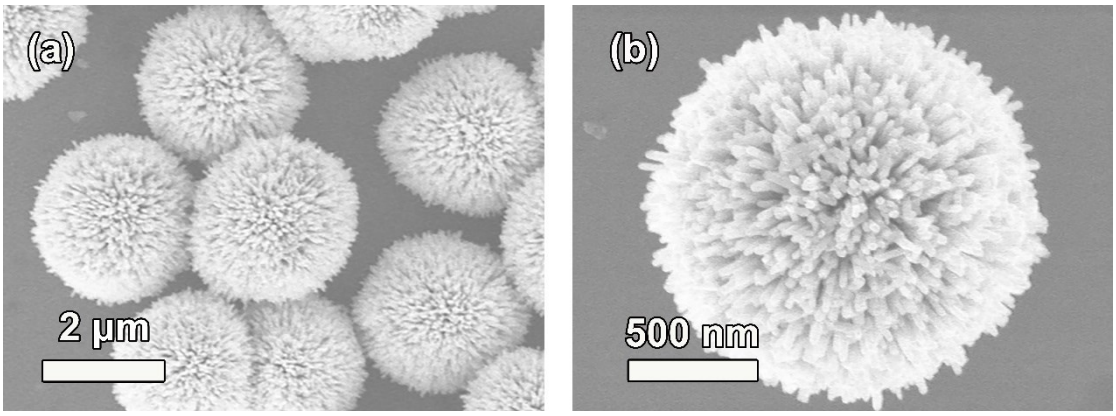

Fig. S2 SEM images of Bi_2S_3 sample prepared with the bismuth source concentration of 20 mM.

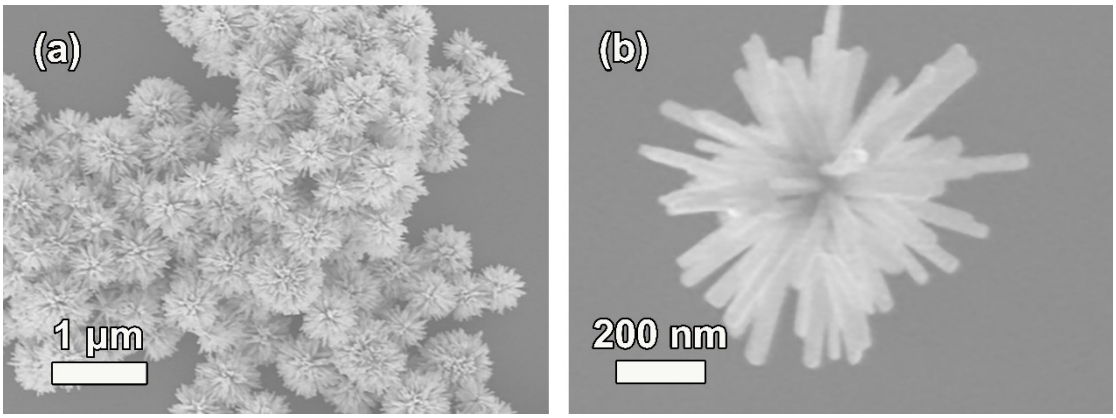

Fig. S3 SEM images of Bi_2S_3 sample prepared with the bismuth source concentration of 5 mM.

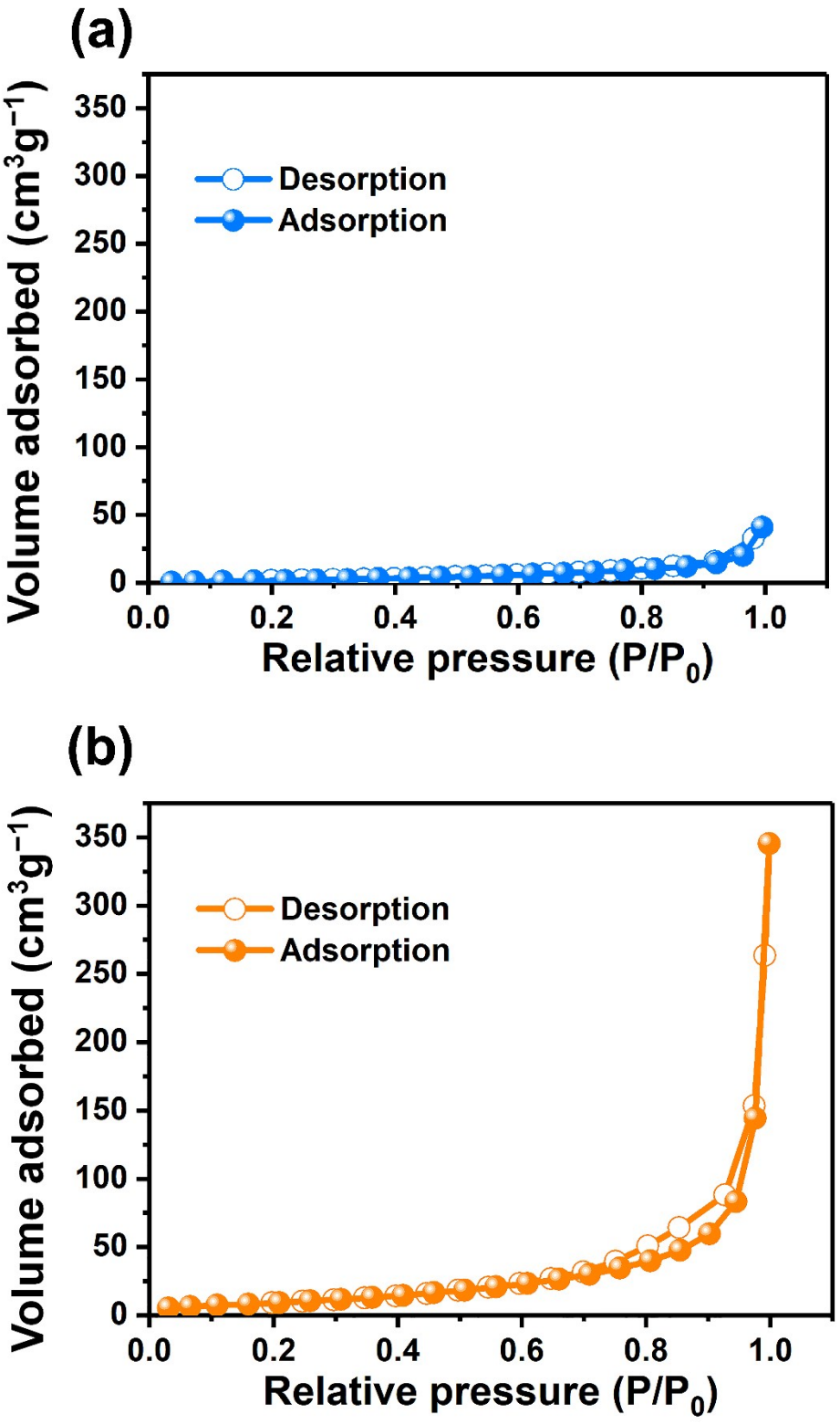

Fig. S4 Nitrogen adsorption-desorption isotherms of (a) self-assembled Bi_2S_3 microspheres, and (b) Bi_2S_3@RGO composite.

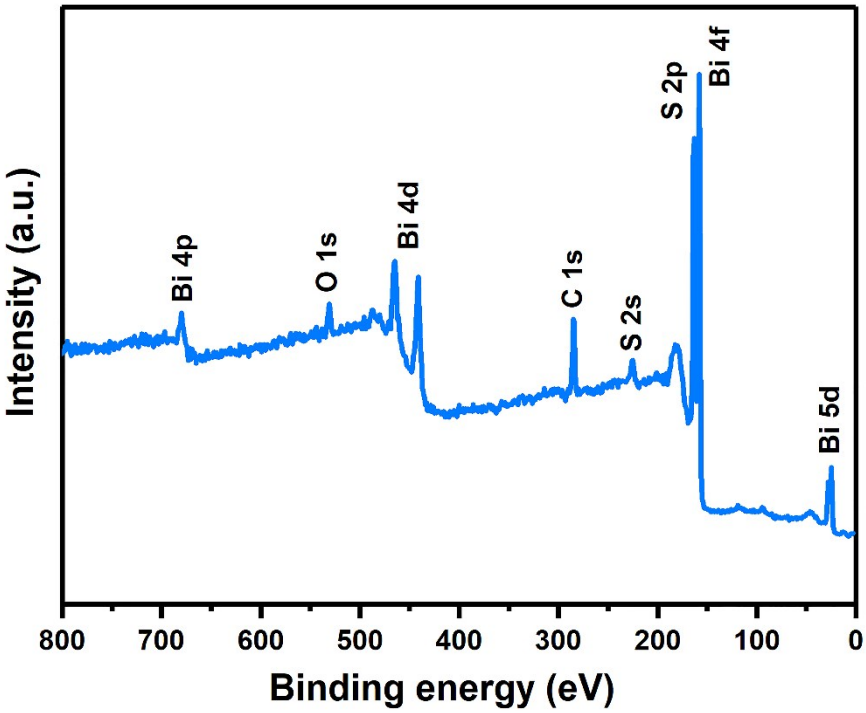

Fig. S5 Survey XPS spectrum of self-assembled Bi_2S_3 microspheres.

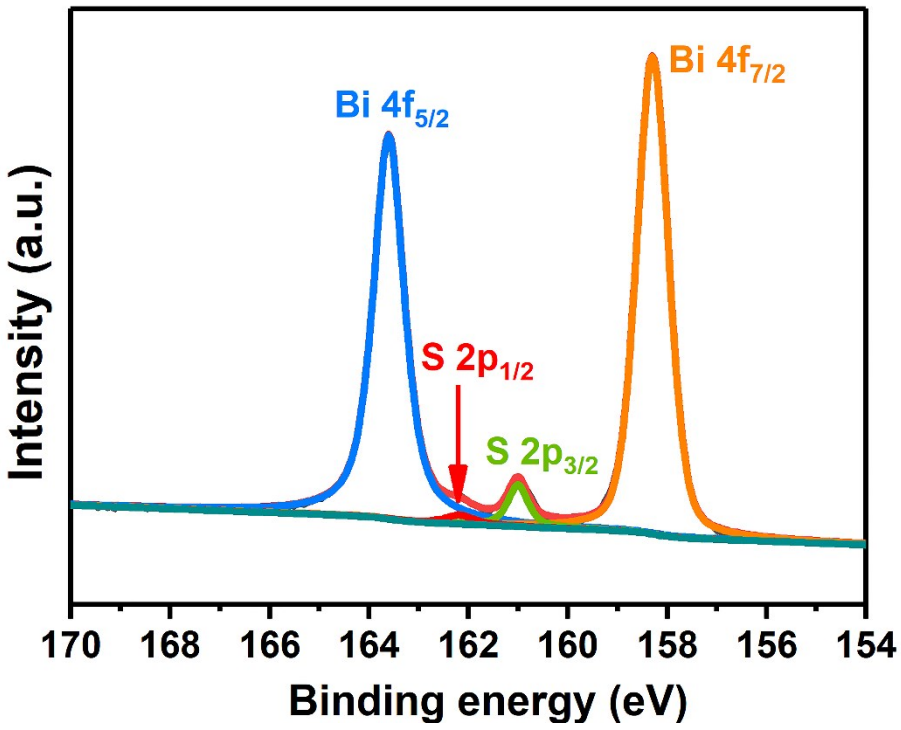

Fig. S6 Bi 4f and S 2p XPS spectra of self-assembled Bi_2S_3 microspheres.

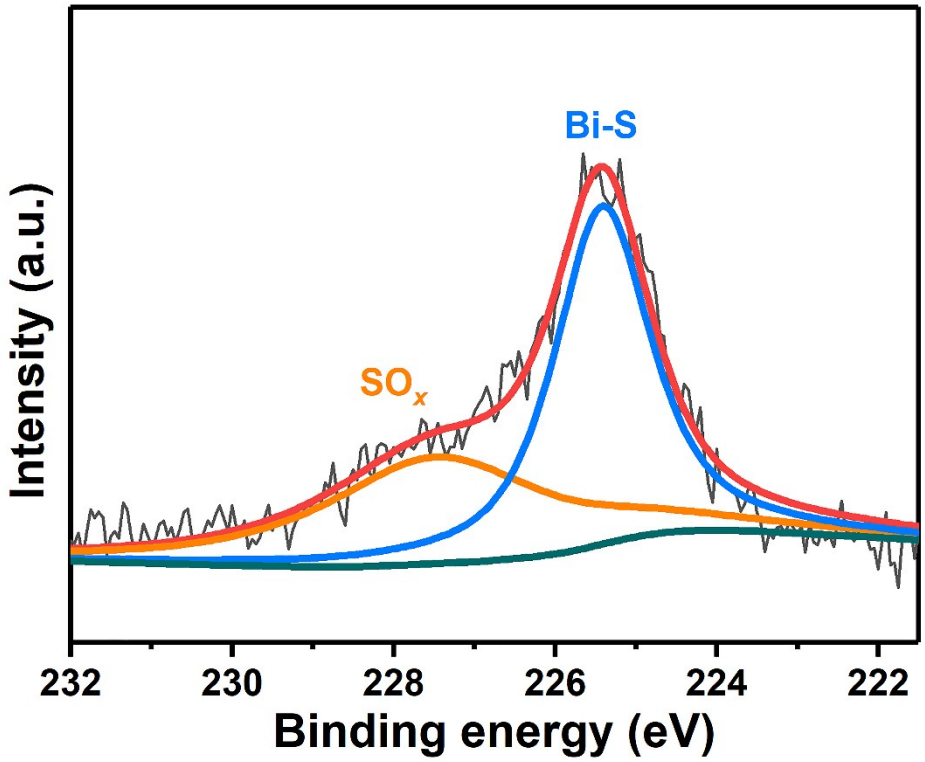

Fig. S7 S 2s XPS spectrum of self-assembled Bi_2S_3 microspheres.

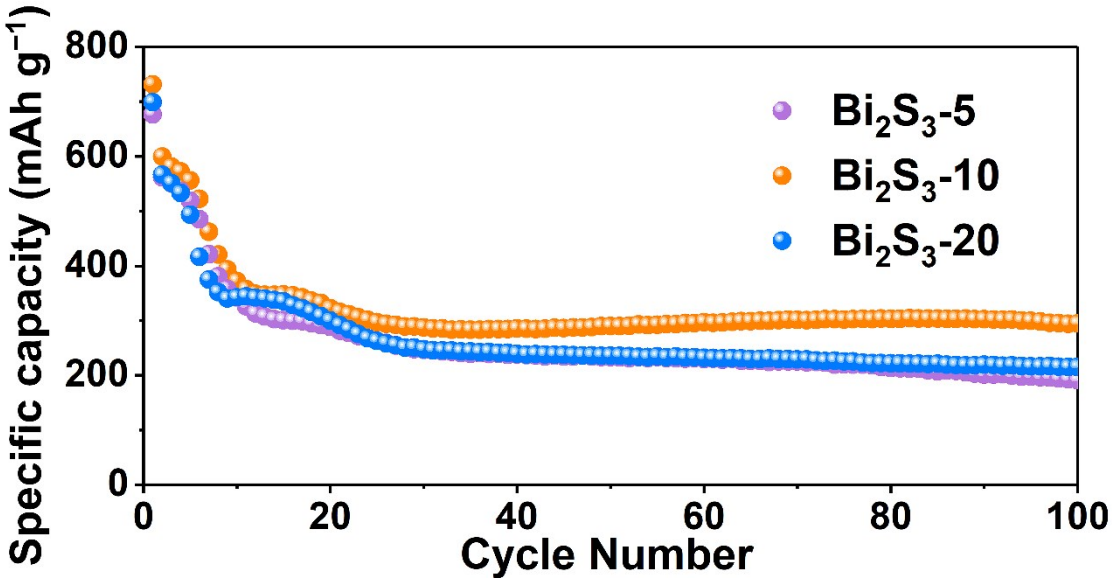

Fig. S8 Cyclic performance of self-assembled Bi_2S_3 microspheres synthesized with different bismuth source concentrations at 2 A g^{-1}. The self-assembled Bi_2S_3 microspheres synthesized with the bismuth source concentrations of 5, 10, and 20 mM are denoted as Bi_2S_3-5, Bi_2S_3-10, and Bi_2S_3-20, respectively.

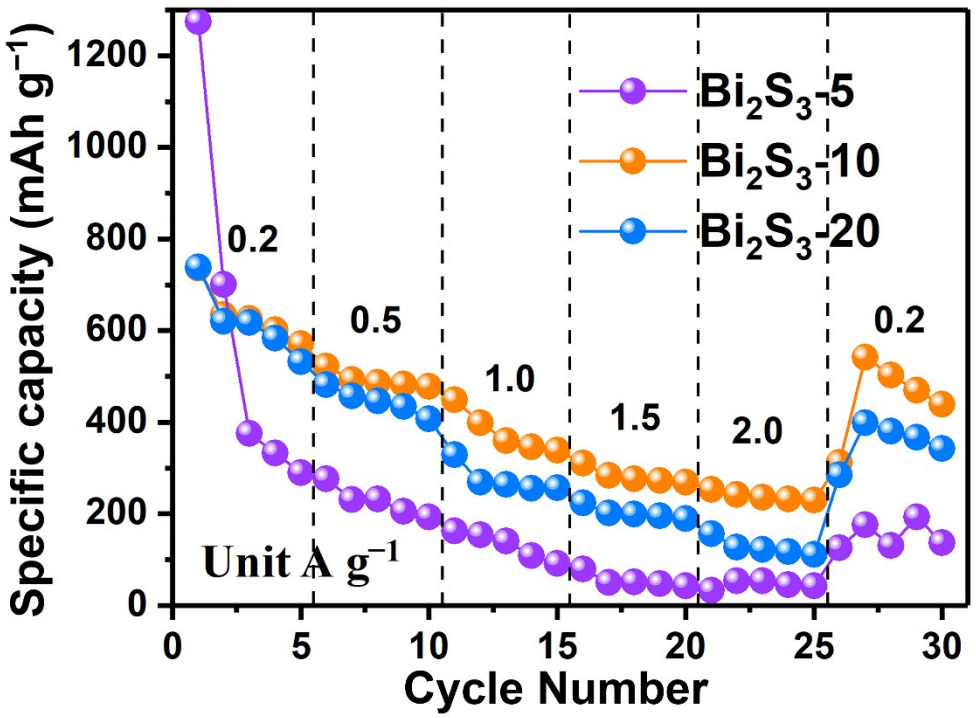

Fig. S9 Rate performance of self-assembled Bi_2S_3 microspheres synthesized with different bismuth source concentrations.

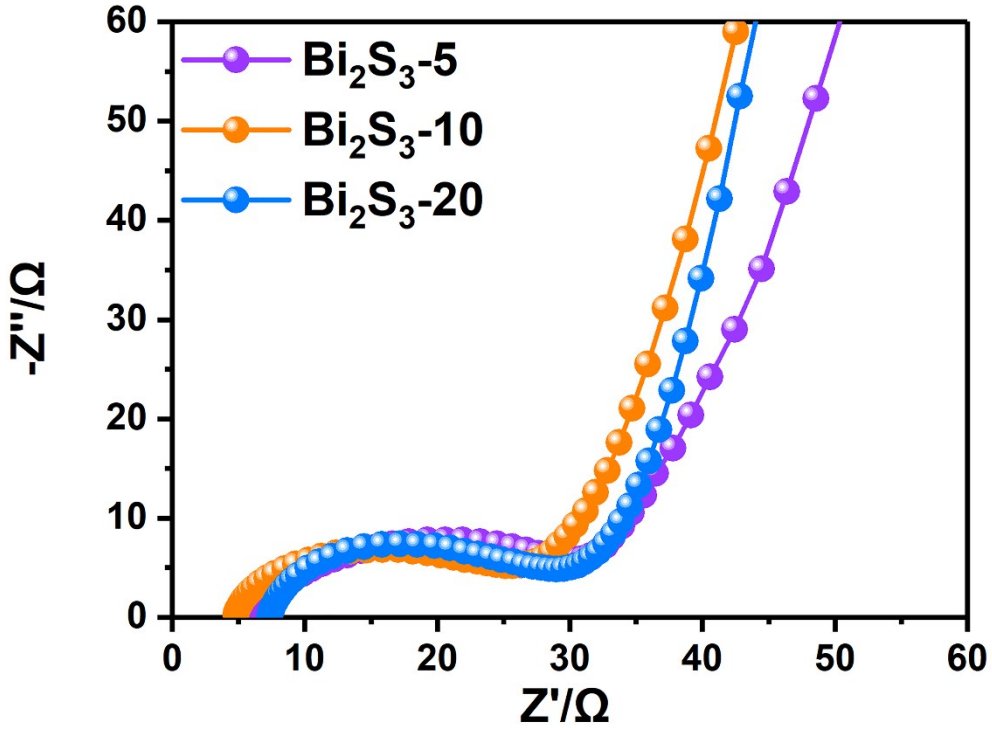

Fig. S10 Nyquist plots of self-assembled Bi_2S_3 microspheres synthesized with different bismuth source concentrations.

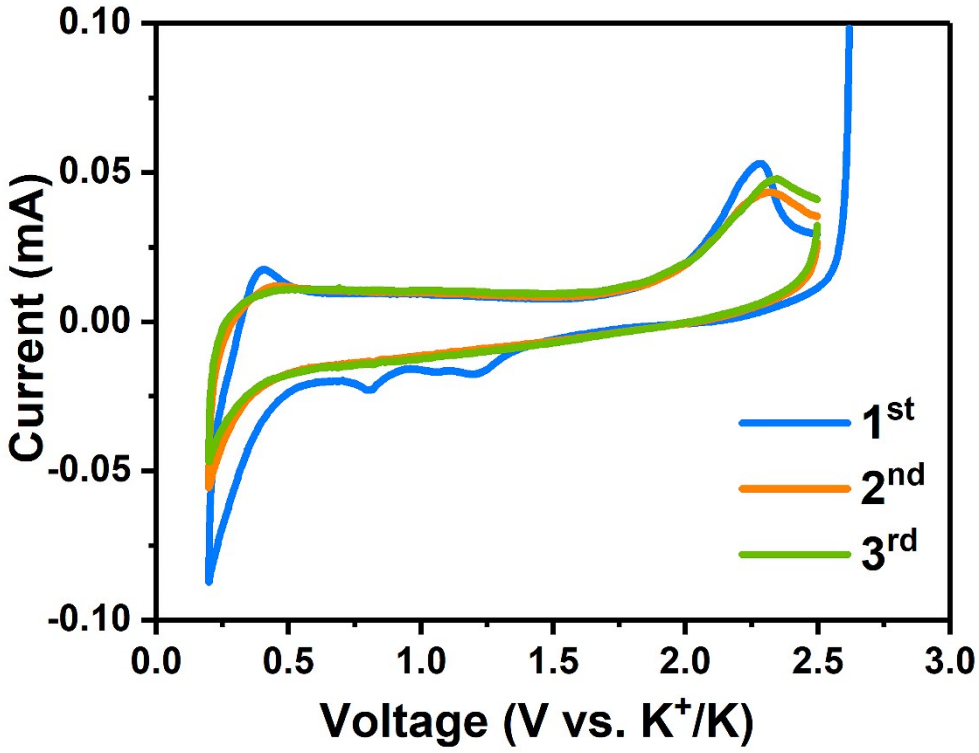

Fig. S11 Cyclic voltammograms of RGO at a scan rate of 0.1 mV s^{-1} in the voltage rage of 0.2-2.5 V.

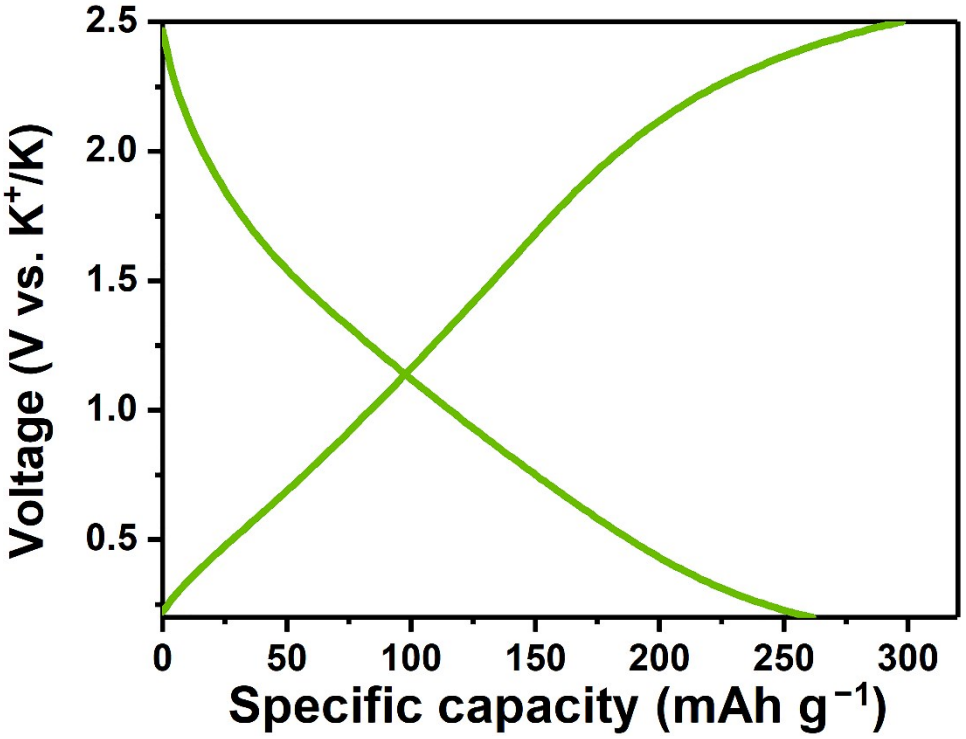

Fig. S12 The 10th galvanostatic charge-discharge curves of RGO at 0.2 A g^{-1} in the voltage rage of 0.2-2.5 V.

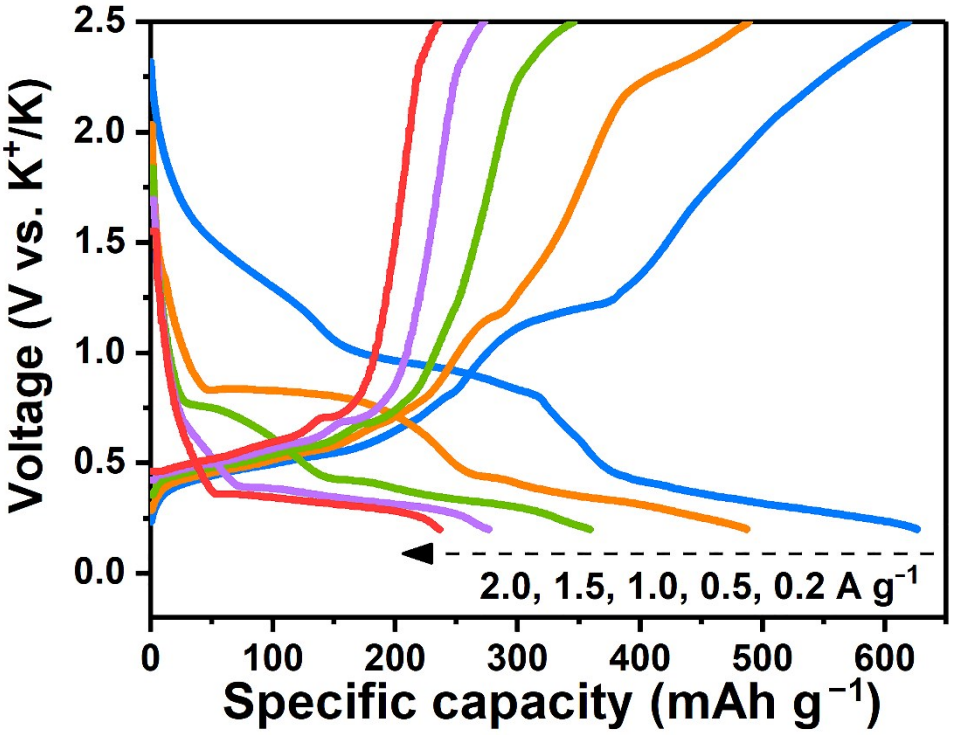

Fig. S13 Galvanostatic charge-discharge curves of self-assembled Bi_2S_3 microspheres at various current densities in the voltage rage of 0.2-2.5 V.

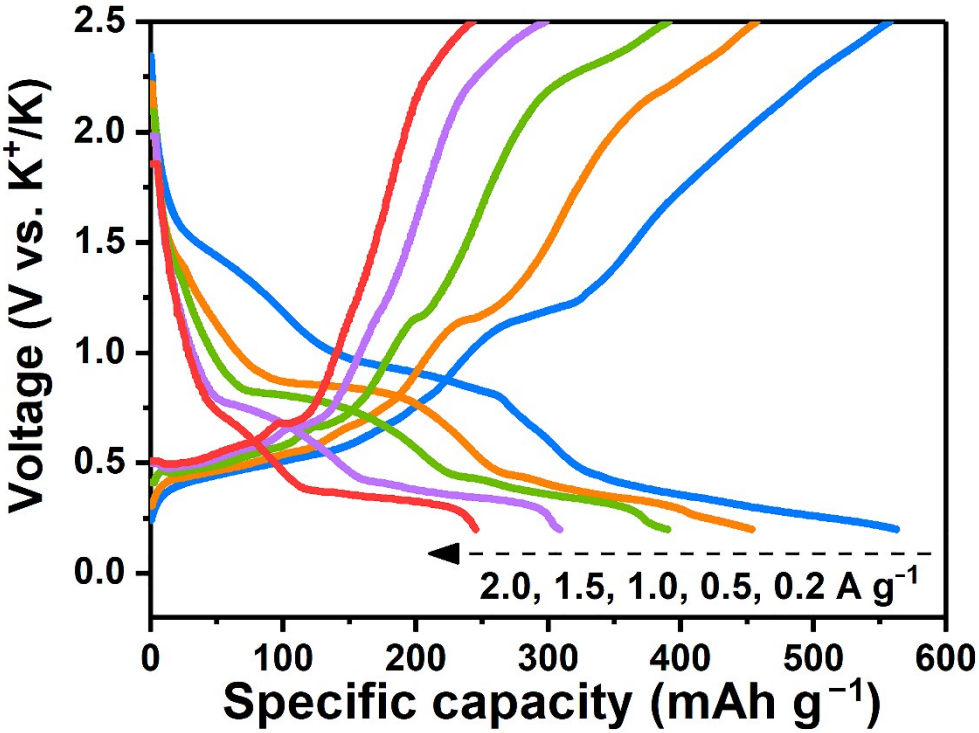

Fig. S14 Galvanostatic charge-discharge curves of Bi_2S_3@RGO composite at various current densities in the voltage rage of 0.2-2.5 V.

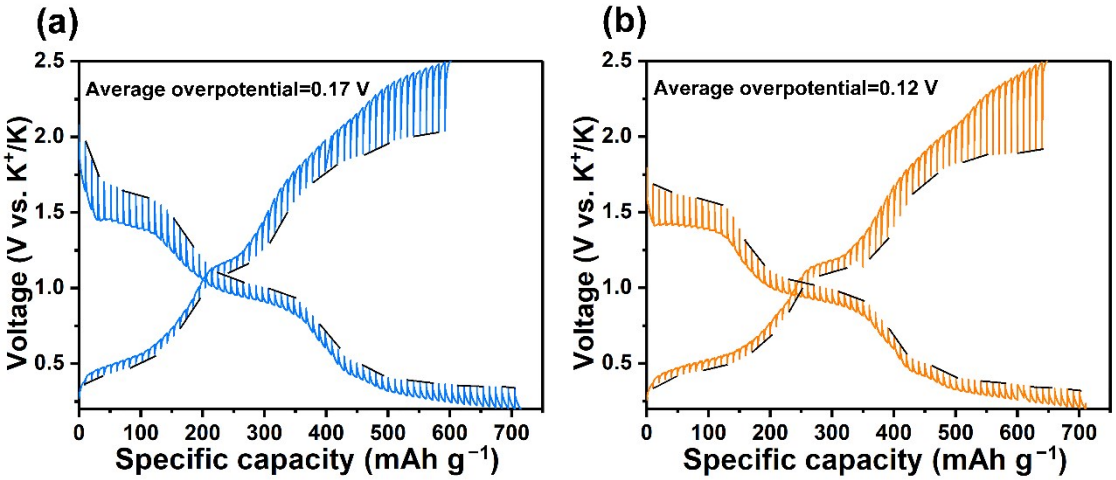

Fig. S15 Galvanostatic intermittent titration technique curves of (a) self-assembled Bi_2S_3 microspheres, and (b) Bi_2S_3@RGO composite.

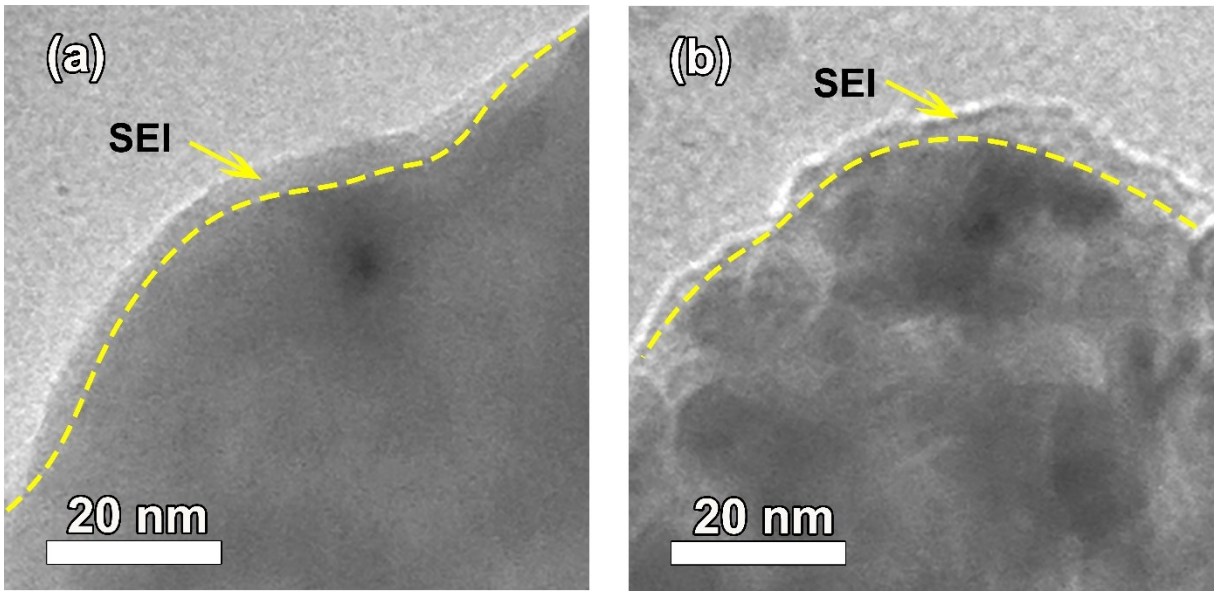

Fig. S16 Ex situ HRTEM image of Bi_2S_3@RGO composite electrode after (b) being discharged to 0.2 V and (c) being charged to 2.5 V.

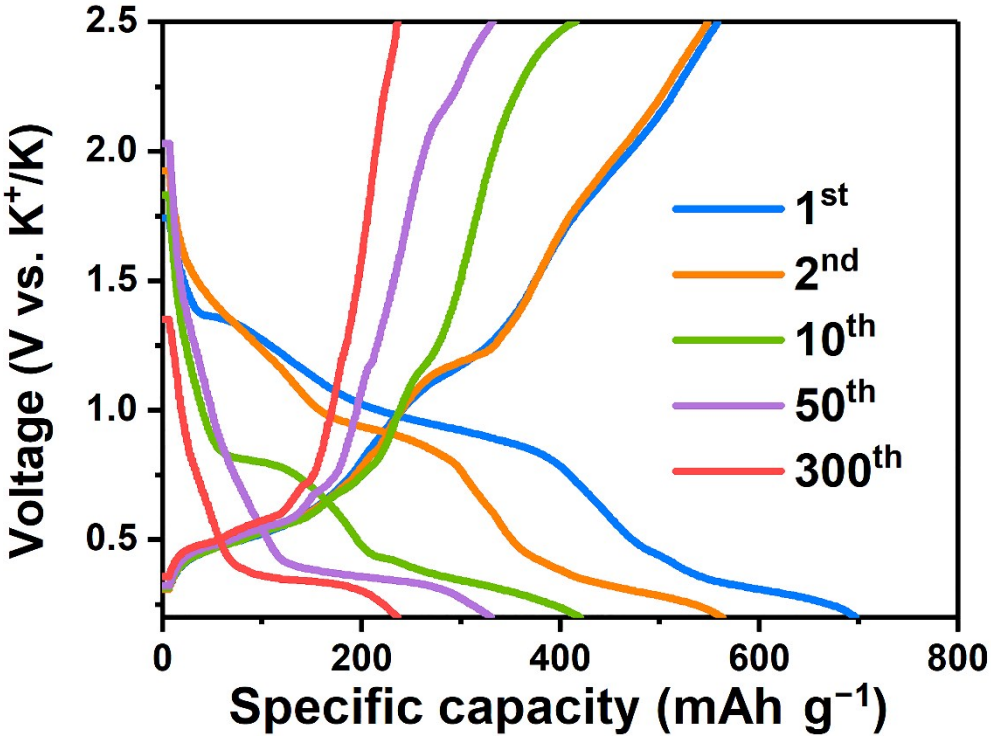

Fig. S17 Galvanostatic charge-discharge curves of Bi_2S_3@RGO composite at 2 A g^{-1} in the voltage rage of 0.2-2.5 V.

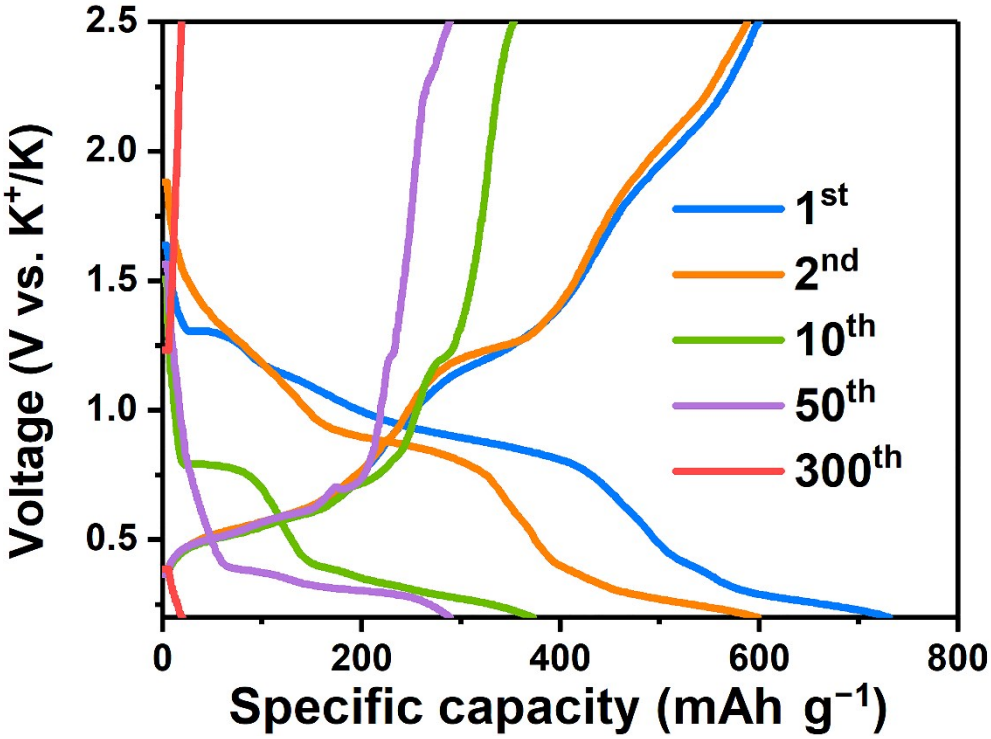

Fig. S18 Galvanostatic charge-discharge curves of self-assembled Bi_2S_3 microspheres at 2 A g^{-1} in the voltage rage of 0.2-2.5 V.

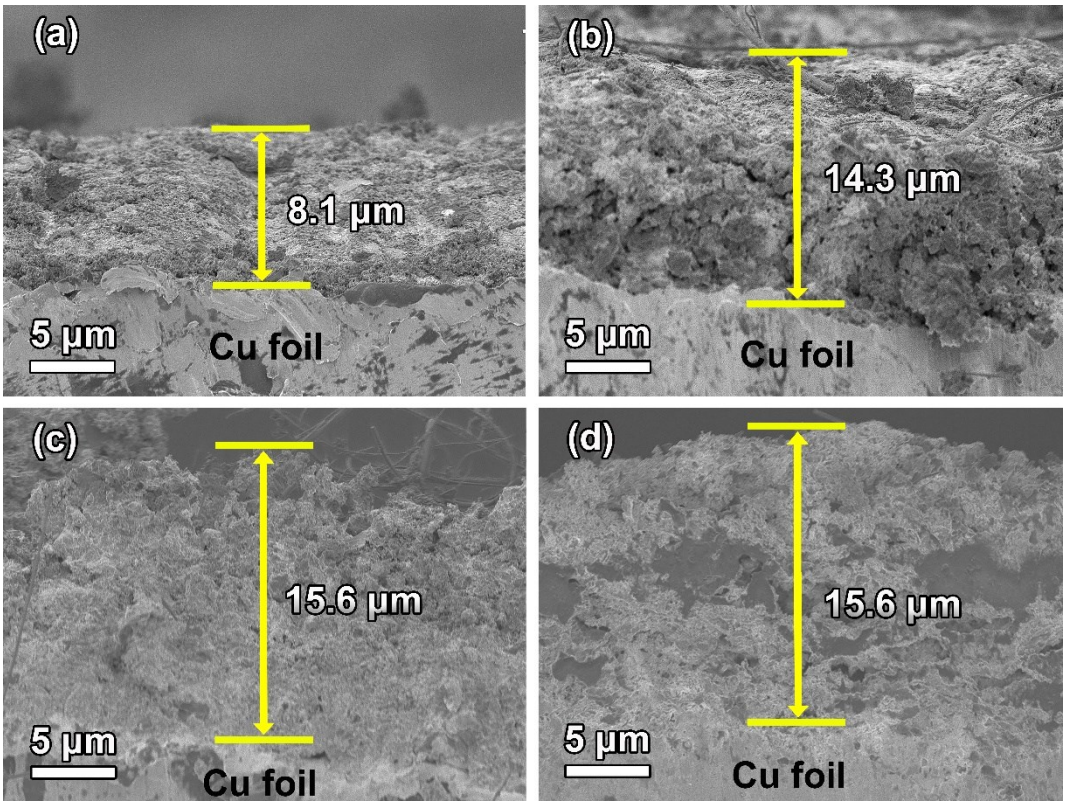

Fig. S19 Cross-section SEM images of the self-assembled Bi_2S_3 microspheres electrodes before (a) and after 30 cycles (b). Cross-section SEM images of the Bi_2S_3@RGO composite electrodes before (c) and after 30 cycles (d).

Table S1 Test data of C H N content of Bi_2S_3@RGO composite.

	C (%)	**H (%)**	**N (%)**
Mean value	7.79	1.064	0.36

Table S2 Test data of electronic conductivity of Bi_2S_3 microspheres and Bi_2S_3@RGO composite.

	Bi_2S_3 (S cm^{-1})	**Bi_2S_3@RGO (S cm^{-1})**
Mean value	0.586	3.67

Table S3 Fitting parameters of electrochemical impedance shown in Fig. 4f in the main text. R_s is solution resistance, R_{ct} is charge transfer resistance.

	R_s (Ω)	**R_{ct} (Ω)**
Bi_2S_3@RGO	5.84	5.26
Bi_2S_3	4.45	16.43

Equivalent circuit

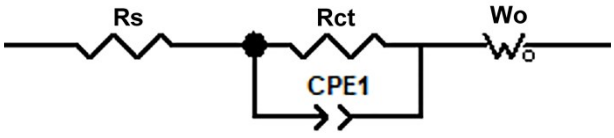

Table S4 The electrochemical-performance parameters of the reported anode materials for PIBs in comparison with this work.

Anode	Capacity		Rate performance			Reference
	Current density (mA g^{-1})	Discharge capacity (mA h g^{-1}	Current density (mA g^{-1})	Discharge capacity (mA h g^{-1})	Cycle number (cycles)	
MoS_2	100	320	1000	183	100	1
MoS_2@MoO_2@Fe@CN	200	317	500	~160	500	2
MoS_2/N-doped-C	200	238	500	151	1000	3
$TiNb_2O_6$@MoS_2/C	200	373	1000	175	300	4
MoS_2@HPCS	200	343.8	1000	126.2	500	5
FeS_2@G@CNF	200	332	1000	120	680	6
AC@CoS/NCNTs/CoS@CNFs	200	381.9	3200	130	600	7
CoS@G	200	~330	500	310.8	100	8
NiS_2@C@C	50	386.8	500	116.9	200	9
NiS@C	200	410	1000	171	300	10
ZSC@C@RGO	200	223	500	208	300	11
VSe_2	100	366	2000	169	500	12
$CoSe_2$/NCNT	200	253	2000	173	600	13
FeP/C	50	288.9	500	178.56	50	14
$MoSe_2$/N-C	100	258.02	1000	197	100	15
SnSb@NC	50	357.2	500	185.8	200	16
$FeSe_2$/NC	100	434	1000	301	250	17
ZnSe@C	200	360	2000	204	100	18
Carbon nanocages (NOGCN)	200	355	500	131	300	19
Nitrogen-doped carbon	100	251.2	1000	101.1	1000	20
Bi_2S_3@RGO	200	538	2000	237	300	This work

References

1 Z. Yu, Y. Xie, B. Xie, C. Cao, Z. Zhang, H. Huo, Z. Jiang, Q. Pan, G. Yin and J. Wang, *Energy Storage Mater.*, 2020, **25,** 416–425.

2 Y. Liu, Y. Xiao, F. Liu, P. Han and G. Qin, *J. Mater. Chem. A*, 2019, **7,** 26818–26828.

3 B. Jia, Q. Yu, Y. Zhao, M. Qin, W. Wang, Z. Liu, C.-Y. Lao, Y. Liu, H. Wu, Z. Zhang and X. Qu, *Adv. Funct. Mater.*, 2018, **28**, 1803409.

4 D. Xing, Q. Yu, B. Jiang, J. Chu, C.-Y. Lao, M. Wang, K. Han, Z. Liu, Y. Bao and W. (A.) Wang, *J. Mater. Chem. A*, 2019, **7**, 5760–5768.

5 J. Hu, Y. Xie, X. Zhou and Z. Zhang, *ACS Appl. Mater. Interfaces*, 2020, **12**, 1232−1240.

6 C. Chen, Y. Yang, X. Tang, R. Qiu, S. Wang, G. Cao and M. Zhang, *Small*, 2019, **15**, 1804740.

7 W. Miao, Y. Zhang, H. Li, Z. Zhang, L. Li, Z. Yu and W. Zhang, *J. Mater. Chem. A*, 2019, **7**, 5504–5512.

8 H. Gao, T. Zhou, Y. Zheng, Q. Zhang, Y. Liu, J. Chen, H. Liu and Z. Guo, *Adv. Funct. Mater.*, 2017, **27**, 1702634.

9 L. Yang, W. Hong, Y. Zhang, Y. Tian, X. Gao, Y. Zhu, G. Zou, H. Hou and X. Ji, *Adv. Funct. Mater.*, 2019, **29**, 1903454.

10 X. Zhao, F. Gong, Y. Zhao, B. Huang, D. Qian, H.-E. Wang, W. Zhang and Z. Yang, *Chem. Eng. J.*, 2020, **392**, 123675.

11 J. Chu, W. Wang, J. Feng, C.-Y. Lao, K. Xi, L. Xing, K. Han, Q. Li, L. Song, P. Li, X. Li and Y. Bao, *ACS Nano*, 2019, **13**, 6906–6916.

12 C. Yang, J. Feng, F. Lv, J. Zhou, C. Lin, K. Wang, Y. Zhang, Y. Yang, W. Wang, J. Li and S. Guo, Adv. Mater., 2018, **30**, 1800036.

13 Q. Yu, B. Jiang, J. Hu, C.-Y. Lao, Y. Gao, P. Li, Z. Liu, G. Suo, D. He, W. (Alex) Wang and G. Yin, Adv. Sci., 2018, **5**, 1800782.

14 W. Li, B. Yan, H. Fan, C. Zhang, H. Xu, X. Cheng, Z. Li, G. Jia, S. An and X. Qiu, ACS Appl. Mater. Interfaces, 2019, **11**, 22364−22370.

15 J. Ge, L. Fan, J. Wang, Q. Zhang, Z. Liu, E. Zhang, Q. Liu, X. Yu and B. Lu, Adv. Energy Mater., 2018, **8**, 1801477.

16 Z. Wang, K. Dong, D. Wang, S. Luo, Y. Liu, Q. Wang, Y. Zhang, A. Hao, C. Shid and N. Zhao, J. Mater. Chem. A, 2019, **7**, 14309–14318.

17 Y. Liu, C. Yang, Y. Lia, F. Zheng, Y. Li, Q. Deng, W. Zhong, G. Wang and T. Liu, Chem. Eng. J., 2020, **393**, 124590.

18 X. Xu, B. Mai, Z. Liu, S. Ji, R. Hu, L. Ouyang, J. Liu and M. Zhu, Chem. Eng. J., 2020, **387**, 124061.

19 Y. Sun, D. Zhu, Z. Liang, Y. Zhao, W. Tian, X, Ren, J. Wang, X. Li, Y. Gao, W. Wen, Y. Huang, X. Li and R. Tai, Carbon, 2020, **167**, 685–695.

20 Z. Qiu, K. Zhao, J. Liu and S. Xia, Electrochimica Acta, 2020, **340**, 135947.